PCCP



PAPER



Cite this: Phys. Chem. Chem. Phys., 2023, 25, 6416

Received 5th July 2022, Accepted 20th January 2023

DOI: 10.1039/d2cp03050k

rsc.li/pccp

Evidence of symmetry breaking in a Gd₂ di-nuclear molecular polymer†

Thilini Ekanayaka, (Da Tao Jiang, (Db Emilie Delahaye, (Dc Olivier Perez, d Jean-Pascal Sutter, (1) *C Duy Le, (10) Alpha T. N'Diaye, (10) Robert Streubel, (10) a Talat S. Rahman ** and Peter A. Dowben **

A chiral 3D coordination compound, [Gd₂(L)₂(ox)₂(H₂O)₂], arranged around a dinuclear Gd unit has been characterized by X-ray photoemission and X-ray absorption measurements in the context of density functional theory studies. Core level photoemission of the Gd 5p multiplet splittings indicates that spin orbit coupling dominates over j-J coupling evident in the 5p core level spectra of Gd metal. Indications of spin-orbit coupling are consistent with the absence of inversion symmetry due to the ligand field. Density functional theory predicts antiferromagnet alignment of the Gd₂ dimers and a band gap of the compound consistent with optical absorption.

1. Introduction

Rare-earth (lanthanide) ions have been of long standing interest in material science because of their luminescence¹⁻³ and magnetic properties.4-6 Many of the rare earth molecular magnets exhibit large magnetic moments and some exhibit large inherent magnetic anisotropy. 4,7-13 For the lanthanide single molecular magnets with large anisotropy, there is growing evidence of magnetic hysteresis at the molecular level.⁸⁻¹³ For the half-filled 4f⁷ electron configurations, as present in gadolinium(π I) and europium(π I), the spin momentum is at a maximum, but in the absence of ligand field effects, the orbital angular momentum is minimal. The absence of orbital angular momentum leads to zero spin-orbital coupling, hence a nondegenerate ground state. 14,15 The electronic structure of Gd and Tb metal is dominated by j-J coupling, 16,17 but this picture may not be strictly applicable to molecular lanthanide systems.

Studies have been undertaken on di-nuclear gadolinium complexes where the di-nuclear unit shows asymmetry resulting

In this study, a 3D coordination compound, [Gd₂(L)₂(ox)₂- $(H_2O)_2$, (where ox corresponds to the oxalate ligand $(C_2O_4)^{2-}$ and L⁻ is a chiral imidazolium ligand bearing two carboxylate groups, Fig. 1), developing from a di-nuclear Gd unit was studied using X-ray photoemission and X-ray absorption spectroscopy techniques. The Gd ions are coupled antiferromagnetically and this type of dinuclear array of lanthanide chains may suitable²⁵ for voltage control in a continuous readout logic gate based on a solid state Mach-Zehnder interferometer. 25-33 In this context, spin orbit coupling would enhance device functionality and performance. 14,25,34 The strong magnetic anisotropy that can be imposed on the Gd ion, by a ligand field, can give rise to different zero-field splittings and thus provide distinct spin qubits in the [Gd₂] molecular dimer.¹⁸

2. Experiment

The [Gd₂(L)₂(ox)₂(H₂O)₂] compound was synthesized by reacting in solvothermal conditions the imidazolium ligand [HL] $(0.530 \text{ g}, 2.50 \text{ mmol}) \text{ with } Gd(NO_3)_3 \cdot 6H_2O (1.128 \text{ g}, 2.5 \text{ mmol})$ and oxalic acid H₂ox (0.157 g, 1.25 mmol) in a mixture water/ ethanol (6 mL, 1:1 vol) at 393 K for 3 days. Crystalline material was filtered and washed with ethanol (yield: 57%). Crystal

in the loss of inversion symmetry. This loss of symmetry occurs from the interaction between the ligands and Gd ions. 18-20 Loss of inversion symmetry is associated with chiral effects and can lead to a large spin orbital coupling. Spin-orbit coupling can play a key role in spintronics leading to topologically protected spin currents,²¹ while an anisotropy barrier and a large moment can play a role in voltage-controlled quantum computing based on molecular magnets. 10,18,22-24

a Department of Physics and Astronomy, Theodore Jorgensen Hall, 855 North 16th Street, University of Nebraska-Lincoln, Lincoln, NE, 68588-0299, USA. E-mail: pdowben1@unl.edu

^b Department of Physics, University of Central Florida, 4000 Central Florida Blvd, Building 121 PS 430, Orlando, FL, 32816, USA. E-mail: talat@ucf.edu

^c Laboratoire de Chimie de Coordination du CNRS (LCC), Université de Toulouse, CNRS. Toulouse. France. E-mail: iean-pascal.sutter@lcc-toulouse.fr

^d Normandie Univ, ENSICAEN, Unicaen, CNRS, CRISMAT, 14000, Caen, France

^e Lawrence Berkeley National Laboratory, Advanced Light Source, Berkeley, CA, 94720, USA

[†] Electronic supplementary information (ESI) available: Structural information and details of the electronic structure calculations. CCDC 2160787. For ESI and crystallographic data in CIF or other electronic format see DOI: https://doi.org/ 10.1039/d2cp03050k

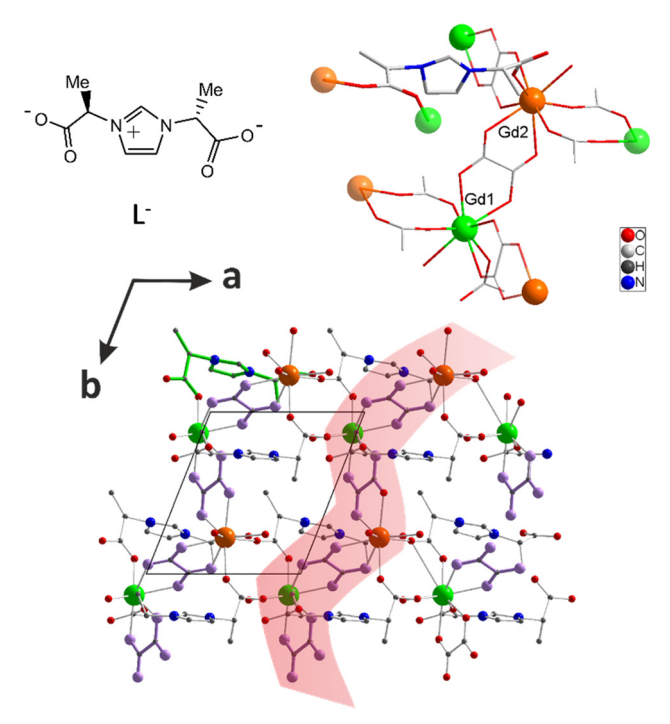


Fig. 1 The crystal structure of $[Gd_2(L)_2(ox)_2(H_2O)_2]$: (top) a schematic of the chiral imidazolium ligand, L⁻, and details of the connectivity between the ligands and the Gd ions (only one L⁻ is fully depicted, for the others only the carboxylic moieties are plotted) where the independent Gd1 and Gd2 sites are shown in green and orange, respectively); (bottom) a view of the 3D organization highlighting the Gd-oxalate chain organization.

structure was studied by X-ray diffraction on single crystal (for further details, see ESI†). Phase purity was confirmed by powder X-ray diffraction (see Fig. S4 in ESI†). Elemental analysis for $[Gd_2(L)_2(ox)_2(H_2O)_2]$ (M = 948.5 g mol⁻¹) found (calc.): C 27.28 (27.83), H 2.70 (2.74), N 5.68 (5.90). Infrared (reflectance, cm⁻¹): 3303 (w), 3132 (w), 3087 (w), 2992 (w), 2947 (w), 1698 (m), 1601 (s), 1461 (m), 1415 (m), 1363 (m), 1313 (m), 1223 (w), 1180 (w), 918 (w), 988 (w), 794 (s), 597 (m), 489 (m).

The X-ray single crystal experiment was carried out on a Rigaku Synergy S four circles diffractometer equipped with an Eiger 1M Dectris detector; a Cu micro focus photonjet X-ray source was used. Low temperature measurements were achieved using an Oxford cryostream 800 system. A schematic representation of the [Gd₂(L)₂(ox)₂(H₂O)₂] compound is shown in Fig. 1 and details on the crystal structure analysis are given in the ESI.† The crystallographic information for the structure has been deposited at CCDC with number 2160787.†

The elemental analysis for C, H, N was carried out at the Laboratoire de Chimie de Coordination using a PerkinElmer 2400 series II instrument. The infrared measurements were done using a PerkinElmer spectrum GX 2000 FT-IR spectrometer. The absorption measurements were done using a PerkinElmer Lambda 950 spectrometer (spectra recorded in reflection mode using a 150 mm integrating sphere with a mean resolution of 2 nm and a sampling rate of 225 nm min⁻¹).

The X-ray absorption spectroscopy (XAS) measurements was performed at the bending magnet beamline 6.3.1, at Advanced

Light Source at Lawrence Berkley National Laboratory and the photon flux was in the region of 1.16 \times 10⁴ photons s⁻¹ μ m⁻² in the two-bunch mode. The absorption across the Gd N2.3 edge was done on electron yield mode. X-ray photoemission spectroscopy (XPS) measurements were taken using nonmonochromatized Al K\alpha X-ray source. The photon energy of 1486.6 eV and SPECS PHOIBOS 150 energy analyzer with photon energy 10 eV was used. All the measurements were taken on the powder.

3. Theory

The orbital-resolved electronic structure of $[Gd_2(L)_2(ox)_2(H_2O)_2]$ was calculated by density functional theory (DFT) employing the projector augmented wave method (PAW) pseudopotentials³⁵ method as implemented in the VASP package. 36,37 The electronic exchange and correlation were accounted with the Perdew-Burke-Ernzerhof (PBE)³⁸ functional with the density functional theory DFT-D3³⁹ correction (with and without Hubbard *U* parameter of 6.8 eV for Gd 4f electron, i.e. PBE+U) and the Heyd-Scuseria-Ernzerhof (HSE06) functional. 40,41 We used a Gaussian smearing method, with σ = 0.1 eV, and sampled the Brillouin zone with a $2 \times 2 \times 2$ Γ -centered grid for lattice parameter optimization, structural relaxation and the partial density of states for the PBE and DFT+U, while for HSE a 1 \times 1 \times 1 Γ -centered grid for the partial density of states was used. Spin-orbit coupling (SOC) effects are included in all electronic structure calculations.

4. Spin-orbit coupling

The X-ray photoemission spectrum of $[Gd_2(L)_2(ox)_2(H_2O)_2]$ is shown in Fig. 2. It shows two main Gd 5p core level features of $5p_{3/2}$ and $5p_{1/2}$ at binding energies of around 23 eV and 27 eV. The energy separation between two main features is about 4 eV which is similar to the expected value for the Gd 5p the spinorbit separation. 16,17,42 These two $p_{1/2}$ and $p_{3/2}$ features of the experimental 5p core level photoemission spectrum exhibits a fine structure splitting that can be fitted with six Gaussian peaks (Fig. 2), as expected when the p core level photoemission spectra is dominated by either L-S coupling or j-I coupling (as schematically indicated in Fig. 2). 16,17

While the multiplet splitting of the photoemission spectrum of the Gd 5p levels occurs due to the half-filled 4f level, in fact, what is observed for $[Gd_2(L)_2(ox)_2(H_2O)_2]$ (Fig. 2) is not the multiplet structure of the 5p core level seen for Gd metal (Fig. 2c), in which the multiplets are dominated by j-J coupling. The $[Gd_2(L)_2(ox)_2(H_2O)_2]$ experimental 5p core level photoemission peak around 22 eV feature exhibits three components with binding energies 19.0 \pm 0.1 eV, 21.9 \pm 0.1 eV, and 23.7 \pm 0.1 eV. The feature around 28 eV has three peaks with binding energies 26.1 \pm 0.1 eV, 27.1 \pm 0.1 eV, and 28.9 \pm 0.1 eV. For Gd metal, and an isolated Gd atom, the photohole created by exciting an electron at 5p level will have an electrostatic interaction with unpaired electrons in the 4f level. It has been showed that the splitting obtained from photoemission

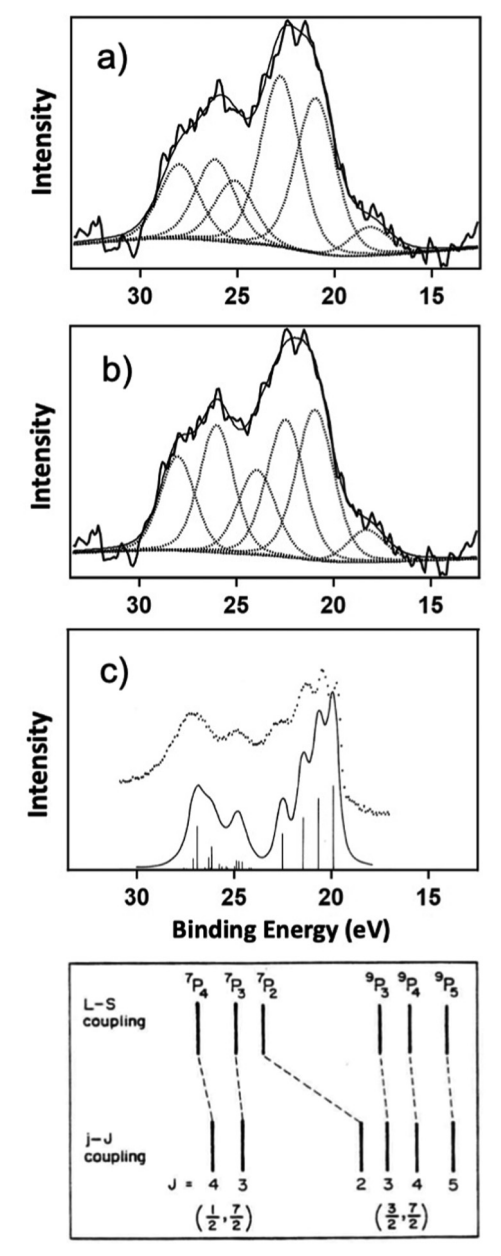


Fig. 2 The X-ray photoemission spectroscopy of Gd, showing the components of the 5p core level components at binding energies of 19.3 eV, 21.9 eV, 23.7 eV, 26.1 eV, 27.1 eV and 28.9 eV, based on an L–S coupling scheme (a), compared to a fitting scheme more in-line with j–J coupling (b) for $[Gd_2(L)_2(ox)_2(H_2O)_2]$. The 5p core level spectra for Gd metal, combined with the multiplets based on configuration interaction calculations, are shown for comparison in (c), taken from ref. 16. Binding energies are with respect to the chemical potential (the Fermi level) in terms of $E_F - E$.

for an Gd atom has a four-fold splitting in the $5p_{3/2}$ feature and concluded that the splitting arises as a result of j–J coupling. ^{16,17} For pure gadolinium, the Gd $5p_{3/2}$ envelope can be fitted with four components at 20.3 eV, 20.9 eV, 22 eV and 23.4 eV and the $5p_{1/2}$ envelope can be fitted with two components at roughly 27.5 eV and 28.3 eV. In other words, the j=3/2 term couples with the $^8S_{7/2}$ to form four multiplets under the Gd $5p_{3/2}$ envelope, because of j–J coupling. ^{16,17} This is not seen here for $[Gd_2(L)_2(ox)_2(H_2O)_2]$.

This is evident in Fig. 2 where the Gd 5d core level is fitted according to a j-J photoemission final state coupling scheme (Fig. 2a), an L-S photoemission final state coupling scheme (Fig. 2b) and the observed j-J photoemission final state coupling scheme (Fig. 2c) seen for Gd metal. 16 Even with the inclusion of the configuration interactions (Fig. 2c), the largest J angular momentum multiplets, that is to say the J = 5 multiplet in the $5p_{3/2}$ Gd core level envelope and the I = 4 multiplet in the $5p_{1/2}$ Gd core level envelope, should be the most intense in the j-J photoemission final state coupling scheme. 16 This is true for Gd metal (Fig. 2c), ¹⁶ but not for $[Gd_2(L)_2(ox)_2(H_2O)_2]$, as is evident when we attempt to fit the 5p core level spectra to an L-S coupling scheme, as done in Fig. 2b. In this context, we cannot reconcile the j-J photoemission final state coupling scheme to the observed the $5p_{3/2}$ and $5p_{1/2}$ Gd core level photoemission features for [Gd₂(L)₂(ox)₂(H₂O)₂].

The ground state configuration of Gd is $5s^25p^64f^75d^16s^2$, but since in the valence state of gadolinium is nominally 3+, the already weak interaction of the 5d and 6s with the Gd 4f⁷ and 5p⁶ can be ignored. Photoemission from the Gd 5p core leave $5p^{5}4f^{7}$, thus resulting in the ${}^{7}P_{4}$ (28.9 \pm 0.1 eV), ${}^{7}P_{3}$ (27.1 \pm 0.1 eV), and $^{7}P_{2}$ (26.1 \pm 0.1 eV) multiplets under the Gd $5p_{1/2}$ envelope and ${}^{9}P_{3}$ (23.7 \pm 0.1 eV), ${}^{9}P_{4}$ (21.9 \pm 0.1 eV) and ${}^{9}P_{5}$ (19.0 \pm 0.1 eV) under the Gd 5p_{3/2} envelope, as seen in the fitting of Fig. 2. The j-J photoemission final state coupling scheme is not excluded as the multiplets for any large Z system cannot be completely described by L-S coupling or j-J coupling alone. Clearly the situation here, for $[Gd_2(L)_2(ox)_2(H_2O)_2]$, is that L–S coupling dominates if only because the J = 5 multiplet in the 5p_{3/2} Gd core level envelope has a very weak intensity compared to the other multiplets. We note that this analysis here does not include all the various configuration interactions, 16,43-45 which are indeed expected for gadolinium. 16 While some of the components have binding energies that overlap with the O 3s core level, 46 the cross-section for this oxygen core level is very weak and the O 3s core level components are much broader that the features seen here. Even if there are C 3s and O 3s contributions to the Gd 5p core level spectra seen here (Fig. 2), the multiplets still must be dominated by L–S rather than j–J in the final state of photoemission. If the features at 19.0 \pm 0.1 eV and 28.9 \pm 0.1 eV are wholly due to C 3s and O 3s contributions, the results still are easier to reconcile with L-S coupling. While in the scenario the ⁹P₅ multiplet would be assigned to the 23.7 \pm 0.1 eV component, but in this case the Gd 5p_{3/2} envelope has equal width to the Gd $5p_{1/2}$ envelope, which only occurs if L-S coupling dominates.

For the Gd compound studied here, $[Gd_2(L)_2(ox)_2(H_2O)_2]$, the three-fold splitting obtained for both the $5p_{3/2}$ and $5p_{1/2}$ features indicates that the 5p core level photoemission is dominated by L–S coupling. 16,17 Strong L–S coupling, resulting in the 5p core level $^7P_{2,3,4}$ and $^9P_{3,4,5}$ final states, seen here in Fig. 2, is consistent with the local structure around each Gd atom, summarized in more detail in the ESI.† Strong spinorbital coupling, as indicated by the XPS multiplet structure, will arise from symmetry breaking associated with the bonding environment. If there is no inversion symmetry, spin-orbit

coupling is turned on and can be seen in photoemission. In compounds, especially with more ionic bonds, the core level photoemission multiplets can be more dominated by L-S coupling than j-J coupling. 45,47 So the trend towards L-S is expected, especially if inversion symmetry is lost, as indicated by the crystal structure of Fig. 1. This is also consistent with the much broader Gd 5p envelope seen in core level photoemission of $[Gd_2(L)_2(ox)_2(H_2O)_2]$ compared to Gd metal, as seen in Fig. 2. The anisotropy of the multiplet intensities indicates some preferential selection of the specific m_1 states indicative of large magnetic moment anisotropy within the ligand field, in agreement with theoretical expectations discussed below. Realistically, because this is a polynuclear complex, exchange coupling matters and quantitatively accurate values of J need to include dynamic correlation effects, which have been neglected as inclusion would require a more extensive consideration of configuration interactions. 48-50

5. Electronic structure and moment ordering

X-Ray absorption measurements were taken at the Gd N₃ edge, as shown in Fig. 3 together with the calculated partial density of states for the 5d orbitals. X-Ray absorption spectroscopy is a partial measure of the unoccupied orbitals of the Gd weighted energy levels of interest. In this case it gives an idea about the unoccupied orbitals with strong Gd weight, but as noted elsewhere, there will be both ligand and metal contributions to the unoccupied molecular orbitals. Indeed, in dinuclear molecular systems, the role of the ligand is significant.⁵¹ To ascertain which unoccupied molecular orbitals contain both metal and ligand weight, XAS has to be combined with other

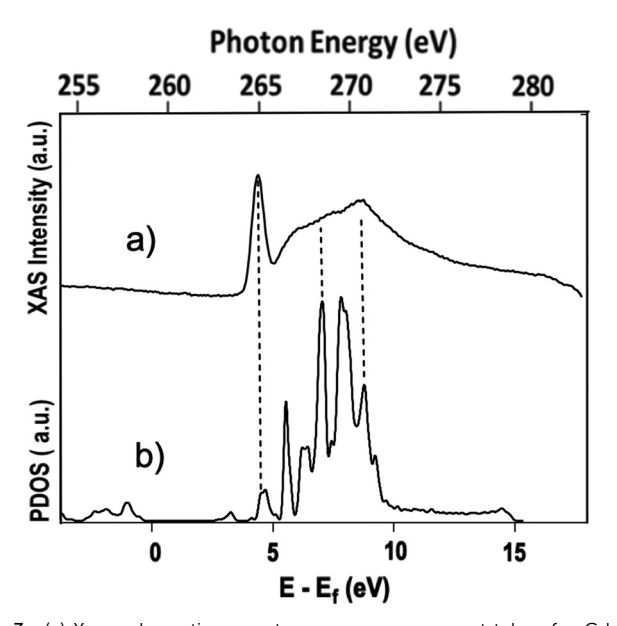


Fig. 3 (a) X-ray absorption spectroscopy measurement taken for Gd N_3 edge. (b) The partial density of states (PDOS) calculated for the Gd 5d contributions to the unoccupied molecular orbitals of $[Gd_2(L)_2(ox)_2(H_2O)_2]$.

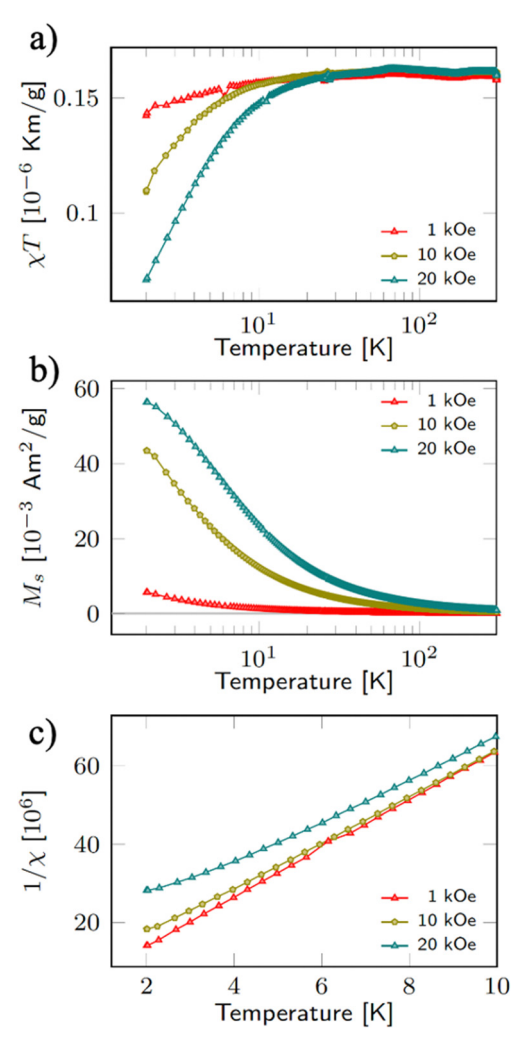


Fig. 4 The product of susceptibility and temperature (a), the saturation magnetization (b), and the inverse DC susceptibility (c) for the warming cycle of 17.9 mg of $[Gd_2(L)_2(ox)_2(H_2O)_2]$.

spectroscopies, 52 which has not been done here. The pre-edge feature of the XAS is around 265 eV which can be identified as one sharp peak and this is followed by a broad spectral signal at higher binding energy region, centered around 270 eV. Since this is a Gd 4p adsorption edge, selection rules are restricted to 4p to 5d and 4p to 6s excitations. As the latter is unlikely and cannot be reconciled with the data in Fig. 3, effectively the XAS in this case is probing the unoccupied density of states with strong 5d weight. This is in qualitative agreement with the calculated Gd 5d partial density of states that contribute to the [Gd₂(L)₂(ox)₂(H₂O)₂] unoccupied molecular orbitals, as shown in Fig. 3b.

The antiferromagnetic coupling between the two localmoment Gd spins was experimentally confirmed by vibrating sample magnetometry using a DynaCool Physical Properties Measurement System (Quantum Design). Fig. 4 shows the saturation magnetization, inverse DC susceptibility, and product of susceptibility and temperature, at different bias fields, for the warming cycle of [Gd₂(L)₂(ox)₂(H₂O)₂]. No difference

between warming and cooling curves was observed. The saturation magnetization increases significantly with the bias field and decreasing temperature. At around 10 K, the curvature of the M(H) curves changes from positive (paramagnetism) to negative (ferro-/antiferromagnetism) with decreasing temperature indicating the presence of antiferromagnetic Gd-Gd interactions. A closer look at the inverse DC susceptibility and the product of susceptibility and temperature allows us to differentiate between paramagnetism ($T_0 = 0$ K), ferromagnetism $(T_0 > 0 \text{ K})$ and antiferromagnetism $(T_0 < 0 \text{ K})$ leveraging the Curie-Weiss law $\chi = C/(T - T_0)$. From a comparison of the inverse susceptibility and magnetization, the antiferromagnetic character of $[Gd_2(L)_2(ox)_2(H_2O)_2]$ is apparent (Fig. 4 and ESI†). Smaller bias fields enable a quantification of the exchange interaction $J_{\text{Gd-Gd}} = -(9 \pm 1) \times 10^{-3} \text{ cm}^{-1}$ and saturation magnetization $14.7\mu_B$ for the Gd(III)₂ molecules at 1.8 K (see ESI†).

Our density functional theory (DFT) show that the antiferromagnetic interaction between the two adjacent Gd atoms has a slightly lower total energy (roughly 3 meV per Gd atom) than a ferromagnetic interaction, as indicated in the schematic Fig. 5a.

This is consistent with the product of susceptibility and temperature data just discussed. The Gd moment is about the same in both cases, i.e. ferromagnetic and antiferromagnetic with similar calculated moments of approximately 6.8, 7.0, and $6.9\mu_{\rm B}$ per Gd atom as predicted by PBE, PBE+U, and HSE exchange correlation functionals, respectively. Although these values for the calculated moments are smaller than that of Gd metal (7.3 μ_B), these calculated moments are consistent with the local moment of $6.7\mu_{\rm B}$ per Gd atom in the compounds GdGa₃₅N₃₆, Gd₂Ga₃₄N₃₆ and GdCGa₃₅N₃₅⁵³ and consistent with a spin moment resulting from 7 unpaired 4f electron spins. We also found that the total number of Gd 5d electrons in this compound is much less than 1e, i.e., the number of 5d electrons in the isolated Gd atom. The total number of Gd 5d electrons calculated with PBE, PBE+U, and HSE06 are 0.60e, 0.58e, and 0.55e, respectively, and total magnetization contributed from d electrons (projected on m_z) are 0.035, 0.034, $0.025\mu_{\rm B}$, respectively.

From the Tauc plot^{54,55} of the optical absorption shown in Fig. 5b, we estimated the optical gap for $[Gd_2(L)_2(ox)_2(H_2O)_2]$ to be indirect and in the region of 2.4 eV (taking r = 2 in $(\alpha h\nu)^{1/r}$ in

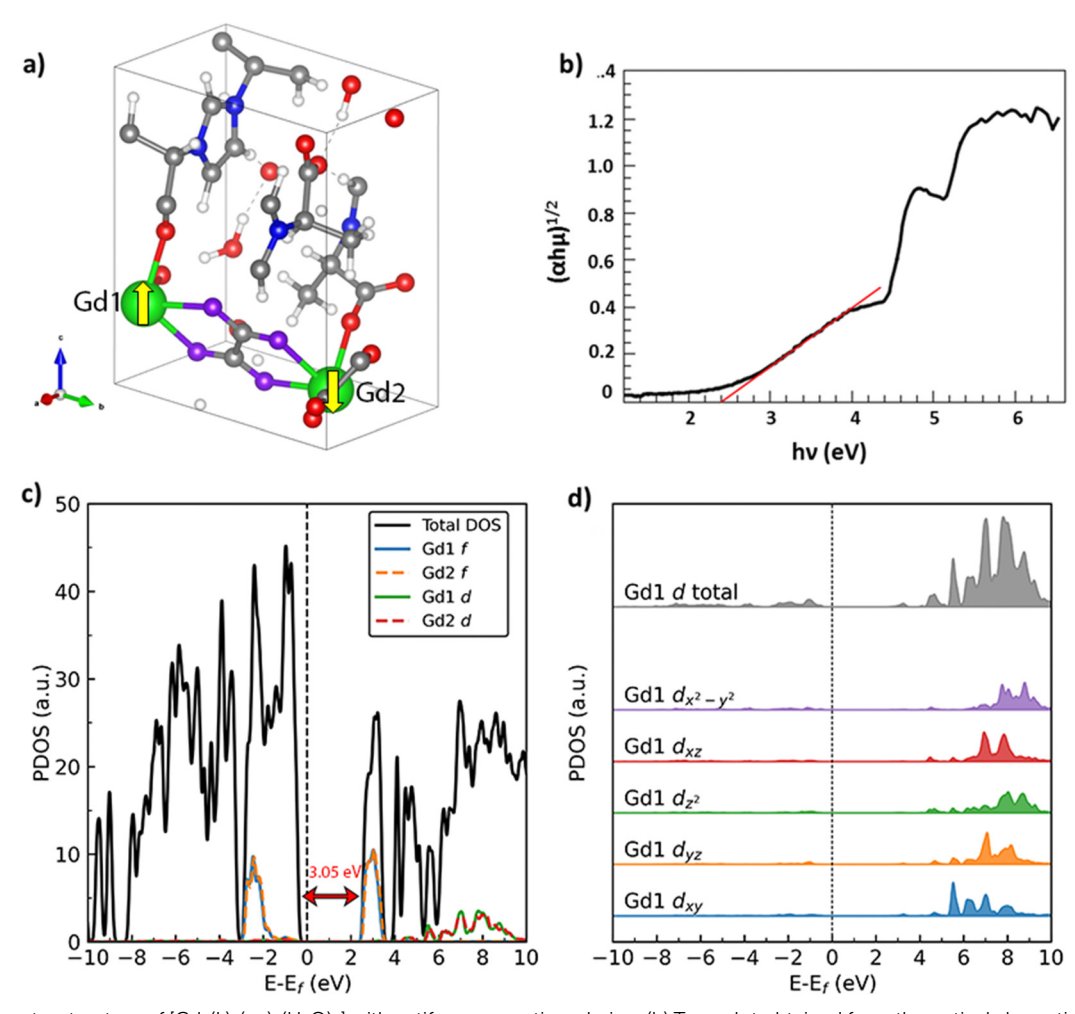


Fig. 5 (a) Geometry structure of $[Gd_2(L)_2(ox)_2(H_2O)_2]$ with antiferromagnetic ordering. (b) Tauc plot obtained from the optical absorption measurements to calculate the optical bandgap. (c) Calculated band gap values. (d) Partial Gd density of states calculated for Gd 5d contributions to the $[Gd_2(L)_2(ox)_2(H_2O)_2]$ orbitals.

the fitting to the optical absorption plot). 50,51 The band gap is smaller than the value calculated from DFT, i.e. 3.05, 3.81, and 5.15 eV calculated with PBE, PBE+U, and HSE06 exchangecorrelation functional (ESI,† Fig. S5). The direct gap (when use r = 1/2 in $(\alpha h \nu)^{1/r}$, $^{54-56}$ from optical absorption is however larger at about 4.5 eV.

DFT has provided a basis for assigning the XAS spectra of other molecular magnets to various unoccupied molecular orbitals.⁵² While the comparison of experiment and theory, vis-à-vis the band gaps, provide some minor validation of the efficacy of the density functional theory, from a comparison of theory to the X-ray absorption, as seen in Fig. 3, it is clear that the excitation from the 4p_{3/2} to unoccupied Gd 5d weighted unoccupied orbitals (plotted in Fig. 5d) is dominated by $p_{x,y}$ to 5d d_{xz} , $d_{x^2-y^2}$ and d_{xy} . The strong spectral weight in XAS, at the adsorption edge is well resolved and separated from the broad Gd 5d weighted unoccupied orbitals contribution. If all Gd 5d weighted unoccupied orbitals, the edge feature would not be so pronounced. If the broad XAS feature is then the result of transitions to the Gd 5d d_{xz} , and $d_{x^2-y^2}$ or 5d d_{xz} and d_{z^2} . The edge then must arise from the Gd 5d dxy, based on the DFT (Fig. 5). With this assignment of the XAS edge, the broad XAS feature is more likely coming from the Gd 5d d_{xz} , and $d_{x^2-v^2}$ unoccupied molecular orbitals given the XAS line shape.

6. Conclusions

Large spin orbit coupling is inferred from the 5p core multiplets seen in X-ray photoemission and distinguishes [Gd₂(L)₂(ox)₂-(H₂O)₂] from the gadolinium atom and gadolinium metal^{16,17} where j-J coupling dominates. The origin of the unusual L-S coupling in the Gd atoms of $[Gd_2(L)_2(ox)_2(H_2O)_2]$ is indicative of a loss of inversion symmetry due to the local bonding about each Gd atom and is consistent with the local structure. DFT calculations suggest that antiferromagnetic interactions are favoured while a comparison of theory with experiment indicated that the X-ray absorption at the 4p_{3/2} core is dominated by excitations from $p_{x,y}$ to 5d $d_{x^2-y^2}$ and d_{xy} . We anticipate that [Gd₂(L)₂(ox)₂(H₂O)₂] will exhibit chiral optical effects where incident circularly polarized light could generate topologically protected spin photocurrents.

Conflicts of interest

There are no conflicts to declare.

Acknowledgements

This research was supported by the National Science Foundation through NSF-DMR 2003057 [T. Ekanayaka and P. A. Dowben] and the EPSCoR RII Track-1: Emergent Quantum Materials and Technologies (EQUATE), Award OIA-2044049 [R. Streubel]. Use of the Advanced Light Source, Lawrence Berkeley National Laboratory, was supported by the US Department of Energy (DOE) under contract no. DE-AC02-05CH11231.

DFT works are supported in part by US DOE under grant DE-FG02-07ER46354 and are performed at the National Energy Research Scientific Computing Center (NERSC). The authors acknowledge Guanhhua Hao for technical support. E. Delahaye thanks the CNRS and the Agence Nationale de la Recherche (ANR contracts no. ANR-15-CE08-0020-01) for funding. The authors would like to thank Archit Dhingra for some helpful

References

- 1 S. Sato, A. Ishii, C. Yamada, J. Kim, C. Ho Song, A. Fujiwara, M. Takata and M. Hasegawa, Luminescence of fusion materials of polymeric chain-structured lanthanide complexes, Polym. J., 2015, 47, 195-200.
- 2 J.-C. G. Bünzli and S. V. Eliseeva, Intriguing aspects of lanthanide luminescence, Chem. Sci., 2013, 4, 1939.
- 3 S. V. Eliseeva and J.-C. G. Bünzli, Lanthanide luminescence for functional materials and bio-sciences, Chem. Soc. Rev., 2010, 39, 189-227.
- 4 C. Benelli and D. Gatteschi, Magnetism of Lanthanides in Molecular Materials with Transition-Metal Ions and Organic Radicals, Chem. Rev., 2002, 102, 2369-2388.
- 5 C. M. Zaleski, E. C. Depperman, J. W. Kampf, M. L. Kirk and V. L. Pecoraro, Synthesis, Structure, and Magnetic Properties of a Large Lanthanide-Transition-Metal Single-Molecule Magnet, Angew. Chem., 2004, 116, 4002-4004.
- 6 H. Kurzen, L. Bovigny, C. Bulloni and C. Daul, Electronic structure and magnetic properties of lanthanide 3+ cations, Chem. Phys. Lett., 2013, 574, 129-132.
- 7 M. L. Kahn, J.-P. Sutter, S. Golhen, P. Guionneau, L. Ouahab, O. Kahn and D. Chasseau, Systematic Investigation of the Nature of The Coupling between a Ln(III) Ion (Ln = Ce(III) to Dy(III)) and Its Aminoxyl Radical Ligands. Structural and Magnetic Characteristics of a Series of {Ln(organic radical)₂} Compounds and the Related {Ln(Nitrone)₂} Derivatives, J. Am. Chem. Soc., 2000, 122, 3413-3421.
- 8 J. Luzon and R. Sessoli, Lanthanides in molecular magnetism: so fascinating, so challenging, Dalton Trans., 2012, 41, 13556.
- 9 D. N. Woodruff, R. E. P. Winpenny and R. A. Layfield, Lanthanide Single-Molecule Magnets, Chem. Rev., 2013, **113**, 5110-5148.
- 10 K. Najafi, A. L. Wysocki, K. Park, S. E. Economou and E. Barnes, Toward Long-Range Entanglement between Electrically Driven Single-Molecule Magnets, J. Phys. Chem. Lett., 2019, 10, 7347-7355.
- 11 C. A. P. Goodwin, F. Ortu, D. Reta, N. F. Chilton and D. P. Mills, Molecular magnetic hysteresis at 60 kelvin in dysprosocenium, Nature, 2017, 548, 439-442.
- 12 F.-S. Guo, B. M. Day, Y.-C. Chen, M.-L. Tong, A. Mansikkamäki and R. A. Layfield, Magnetic hysteresis up to 80 kelvin in a dysprosium metallocene single-molecule magnet, Science, 2018, 362, 1400-1403.

- 13 C. A. Gould, K. R. McClain, D. Reta, J. G. C. Kragskow, D. A. Marchiori, E. Lachman, E.-S. Choi, J. G. Analytis, R. D. Britt, N. F. Chilton, B. G. Harvey and J. R. Long, Ultrahard magnetism from mixed-valence dilanthanide complexes with metal-metal bonding, *Science*, 2022, 375, 198–202.
- 14 H. Jang, B. Y. Kang, B. K. Cho, M. Hashimoto, D. Lu, C. A. Burns, C.-C. Kao and J.-S. Lee, Observation of Orbital Order in the Half-Filled 4f Gd Compound, *Phys. Rev. Lett.*, 2016, 117, 216404.
- 15 S. Abdelouahed and M. Alouani, Magnetic anisotropy in Gd, GdN, and GdFe₂ tuned by the energy of gadolinium 4 f states, *Phys. Rev. B: Condens. Matter Mater. Phys.*, 2009, **79**, 054406.
- 16 B. T. Thole, X. D. Wang, B. N. Harmon, D. Li and P. A. Dowben, Multiplet fine structure in the photoemission of the gadolinium and terbium 5 p levels, *Phys. Rev. B: Condens. Matter Mater. Phys.*, 1993, 47, 9098–9101.
- 17 D. Li, P. A. Dowben and M. Onellion, Multiplet Fine Structure of the Gd and Tb 5P Levels, *MRS Proc.*, 1991, 231, 107.
- 18 F. Luis, P. J. Alonso, O. Roubeau, V. Velasco, D. Zueco, D. Aguilà, J. I. Martínez, L. A. Barrios and G. Aromí, A dissymmetric [Gd₂] coordination molecular dimer hosting six addressable spin qubits, *Commun. Chem.*, 2020, 3, 176.
- 19 L. E. Roy and T. Hughbanks, Magnetic Coupling in Dinuclear Gd Complexes, *J. Am. Chem. Soc.*, 2006, **128**, 568–575.
- 20 A. Dei, D. Gatteschi, C. A. Massa, L. A. Pardi, S. Poussereau and L. Sorace, Spontaneous Symmetry Breaking in the Formation of a Dinuclear Gadolinium Semiquinonato Complex: Synthesis, High-Field EPR Studies, and Magnetic Properties, *Chem. Eur. J.*, 2000, **6**, 4580–4586.
- 21 P. A. Dowben, C. Binek, K. Zhang, L. Wang, W.-N. Mei, J. P. Bird, U. Singisetti, X. Hong, K. L. Wang and D. Nikonov, Towards a Strong Spin-Orbit Coupling Magnetoelectric Transistor, *IEEE J. Explor. Solid-State Comput. Devices Circuits*, 2018, 4, 1–9.
- 22 S. Thiele, F. Balestro, R. Ballou, S. Klyatskaya, M. Ruben and W. Wernsdorfer, Electrically driven nuclear spin resonance in single-molecule magnets, *Science*, 2014, 344, 1135–1138.
- 23 C. Godfrin, A. Ferhat, R. Ballou, S. Klyatskaya, M. Ruben, W. Wernsdorfer and F. Balestro, Operating Quantum States in Single Magnetic Molecules: Implementation of Grover's Quantum Algorithm, *Phys. Rev. Lett.*, 2017, 119, 187702.
- 24 G. Aromí, F. Luis and O. Roubeau, in *Lanthanides and Actinides in Molecular Magnetism*, ed. R. A. Layfield and M. Murugesu, Wiley-VCH Verlag GmbH & Co. KGaA, Weinheim, Germany, 2015, pp. 185–222.
- 25 A. Dhingra, X. Hu, M. F. Borunda, J. F. Johnson, C. Binek, J. Bird, A. T. N'Diaye, J.-P. Sutter, E. Delahaye, E. D. Switzer, E. del Barco, T. S. Rahman and P. A. Dowben, "Molecular Transistors as Substitutes for Quantum Information Applications", J. Phys.: Condens. Matter, 2022, 34, 2200238.
- 26 I. Neder, M. Heiblum, Y. Levinson, D. Mahalu and V. Umansky, Unexpected Behavior in a Two-Path Electron Interferometer, *Phys. Rev. Lett.*, 2006, 96, 016804.
- 27 V. S.-W. Chung, P. Samuelsson and M. Büttiker, Visibility of current and shot noise in electrical Mach-Zehnder and

- Hanbury Brown Twiss interferometers, *Phys. Rev. B: Condens. Matter Mater. Phys.*, 2005, 72, 125320.
- 28 D. E. Feldman and A. Kitaev, Detecting Non-Abelian Statistics with an Electronic Mach-Zehnder Interferometer, *Phys. Rev. Lett.*, 2006, **97**, 186803.
- 29 E. Bieri, M. Weiss, O. Göktas, M. Hauser, C. Schönenberger and S. Oberholzer, Finite-bias visibility dependence in an electronic Mach-Zehnder interferometer, *Phys. Rev. B: Condens. Matter Mater. Phys.*, 2009, 79, 245324.
- 30 G. Haack, H. Förster and M. Büttiker, Parity detection and entanglement with a Mach-Zehnder interferometer, *Phys. Rev. B: Condens. Matter Mater. Phys.*, 2010, **82**, 155303.
- 31 D. S. Wei, T. van der Sar, J. D. Sanchez-Yamagishi, K. Watanabe, T. Taniguchi, P. Jarillo-Herrero, B. I. Halperin and A. Yacoby, Mach-Zehnder interferometry using spin-and valley-polarized quantum Hall edge states in graphene, *Sci. Adv.*, 2017, 3, e1700600.
- 32 J. R. Williams, L. DiCarlo and C. M. Marcus, Quantum Hall Effect in a Gate-Controlled p-n Junction of Graphene, *Science*, 2007, 317, 638–641.
- 33 Y. Ji, Y. Chung, D. Sprinzak, M. Heiblum, D. Mahalu and H. Shtrikman, An electronic Mach–Zehnder interferometer, *Nature*, 2003, **422**, 415–418.
- 34 L. Nuccio, M. Willis, L. Schulz, S. Fratini, F. Messina, M. D'Amico, F. L. Pratt, J. S. Lord, I. McKenzie, M. Loth, B. Purushothaman, J. Anthony, M. Heeney, R. M. Wilson, I. Hernández, M. Cannas, K. Sedlak, T. Kreouzis, W. P. Gillin, C. Bernhard and A. J. Drew, Importance of Spin-Orbit Interaction for the Electron Spin Relaxation in Organic Semiconductors, *Phys. Rev. Lett.*, 2013, 110, 216602.
- 35 P. E. Blöchl, Projector augmented-wave method, *Phys. Rev. B: Condens. Matter Mater. Phys.*, 1994, **50**, 17953–17979.
- 36 G. Kresse and J. Furthmüller, Efficient iterative schemes for ab initio total-energy calculations using a plane-wave basis set, *Phys. Rev. B: Condens. Matter Mater. Phys.*, 1996, 54, 11169–11186.
- 37 G. Kresse and J. Hafner, Ab initio molecular dynamics for liquid metals, *Phys. Rev. B: Condens. Matter Mater. Phys.*, 1993, 47, 558–561.
- 38 J. P. Perdew, K. Burke and M. Ernzerhof, Generalized Gradient Approximation Made Simple, *Phys. Rev. Lett.*, 1996, 77, 3865–3868.
- 39 S. Grimme, J. Antony, S. Ehrlich and H. Krieg, A consistent and accurate ab initio parametrization of density functional dispersion correction (DFT-D) for the 94 elements H-Pu, *J. Chem. Phys.*, 2010, **132**, 154104.
- 40 J. Heyd, G. E. Scuseria and M. Ernzerhof, Hybrid functionals based on a screened Coulomb potential, *J. Chem. Phys.*, 2003, **118**, 8207–8215.
- 41 J. Heyd, G. E. Scuseria and M. Ernzerhof, Erratum: "Hybrid functionals based on a screened Coulomb potential" [J. Chem. Phys. 118, 8207 (2003)], *J. Chem. Phys.*, 2006, 124, 219906.
- 42 F. Herman and S. Skillman, *Atomic structure calculations*, Prentice-Hall, Englewood Cliffs, NJ, 1963.

43 P. S. Bagus, A. J. Freeman and F. Sasaki, Prediction of New Multiplet Structure in Photoemission Experiments, Phys. Rev. Lett., 1973, 30, 850-853.

- 44 S. T. Manson, Satellite lines in photoelectron spectra, I. Electron Spectrosc. Relat. Phenom., 1976, 9, 21-28.
- 45 B. D. Hermsmeier, C. S. Fadley, B. Sinkovic, M. O. Krause, J. Jimenez-Mier, P. Gerard, T. A. Carlson, S. T. Manson and S. K. Bhattacharya, Energy dependence of the outer corelevel multiplet structures in atomic Mn and Mn-containing compounds, Phys. Rev. B: Condens. Matter Mater. Phys., 1993, 48, 12425-12437.
- 46 D. A. Zatsepin, D. W. Boukhvalov, A. F. Zatsepin, Y. A. Kuznetsova, M. A. Mashkovtsev, V. N. Rychkov, V. Y. Shur, A. A. Esin and E. Z. Kurmaev, Electronic structure, charge transfer, and intrinsic luminescence of gadolinium oxide nanoparticles: Experiment and theory, Appl. Surf. Sci., 2018, 436, 697-707.
- 47 C. S. Fadley, D. A. Shirley, A. J. Freeman, P. S. Bagus and J. V. Mallow, Multiplet Splitting of Core-Electron Binding Energies in Transition-Metal Ions, Phys. Rev. Lett., 1969, 23, 1397-1401.
- 48 F. Neese, Definition of corresponding orbitals and the diradical character in broken symmetry DFT calculations on spin coupled systems, J. Phys. Chem. Solids, 2004, 65, 781-785.
- 49 C. J. Calzado, C. Angeli, D. Taratiel, R. Caballol and J.-P. Malrieu, Analysis of the magnetic coupling in binuclear complexes. I. Physics of the coupling, J. Chem. Phys., 2002, 116, 2728.

- 50 C. J. Calzado, J. Cabrero, J.-P. Malrieu and R. Caballol, Analysis of the magnetic coupling in binuclear complexes. II. Derivation of valence effective Hamiltonians from ab initio CI and DFT calculations, J. Chem. Phys., 2002, **116**, 3985.
- 51 C. J. Calzado, C. Angeli, D. Taratiel, R. Caballol and J.-P. Malrieu, Analysis of the magnetic coupling in binuclear systems. III. The role of the ligand to metal charge transfer excitations revisited, J. Chem. Phys., 2009, 131, 044327.
- 52 E. Mishra, T. K. Ekanayaka, T. Panagiotakopoulos, D. Le, T. S. Rahman, P. Wang, K. A. McElveen, J. P. Phillips, M. Zaid Zaz, S. Yazdani, A. T. NDiaye, R. Y. Lai, R. Streubel, R. Cheng, M. Shatruk and P. A. Dowben, Electronic structure of cobalt spin-crossover molecules in different environments, Nanoscale, 2023, 15, 2044.
- 53 N. Syed Kaleemullah, S. Ramsubramanian, R. Mohankumar, S. Munawar Basha, M. Rajagopalan and J. Kumar, Magnetic properties of gadolinium and carbon co-doped gallium nitride, Solid State Commun., 2017, 249, 7-11.
- 54 J. Tauc, Optical properties and electronic structure of amorphous Ge and Si, Mater. Res. Bull., 1968, 3, 37-46.
- 55 J. Tauc, R. Grigorovici and A. Vancu, Optical Properties and Electronic Structure of Amorphous Germanium, Phys. Status Solidi B, 1966, 15, 627–637.
- 56 E. A. Davis and N. F. Mott, Conduction in non-crystalline systems V. Conductivity, optical absorption and photoconductivity in amorphous semiconductors, Philos. Mag., 1970, 22, 903-922, DOI: 10.1080/1478643700822106.